Experimental and Theoretical Study of the Far-Infrared Spectra of Monovalent Impurities in Sodium Chloride*

H. F. MACDONALD,† MILES V. KLEIN, AND T. P. MARTIN
Department of Physics and Materials Research Laboratory, University of Illinois, Urbana, Illinois 61801
(Received 19 August 1968)

Low-temperature measurements have been made of the far-infrared absorption due to a number of substitutional monovalent impurities in sodium chloride. The natural Cl^{35} and Cl^{37} isotopes, acting as simple mass defects, result in absorption in the acoustic band and yield information about the phonon frequencies in this region. This method has been utilized to improve Caldwell and Klein's shell-model calculation, and the results have been used to interpret the chemical impurity-induced absorption due to Ag^+, Li^+, K^+, F^-, Br^-, and I^- ions in sodium chloride. Various defect models have been employed, involving a change of mass at the defect site together with changes in the force constants coupling the defect and its immediate neighbors. A simple nearest-neighbor central-force model has been found inadequate to explain the far-infrared spectra over a broad frequency range, and for the potassium and iodine impurities a model involving changes in the Szigeti effective charge of the defect has been used. The various defect models are compared and discussed, and possible improvements outlined.

I. INTRODUCTION

IN this paper we report the results of an investigation of the far-infrared absorption spectra of substitutional monovalent impurities in sodium chloride. Preliminary results of this work for chemical impurities (silver, bromine, and fluorine)[1] and isotopic impurities[2] have been described earlier.

Infrared radiation is absorbed in a large, perfect ionic crystal only by the transverse optic phonon of essentially zero wave vector. This is the only mode of the crystal which couples to the long-wavelength external radiation field and, since it is an eigenstate, there is a δ-function response at its frequency ω_0. When substitutional monovalent impurities are introduced into the crystal the radiation still drives only the $k\simeq 0$, TO phonon, but this is no longer an eigenstate. In addition to the δ-function response at ω_0 continuous absorption, perhaps with resonances, appears in the band-mode region,[3] and localized modes may also occur.[4]

Impurity-induced resonance modes in sodium chloride have been observed both directly, in the far infrared,[5–7] and indirectly, in thermal-conductivity measurements.[8,9] The thermal-conductivity curves of crystals containing monovalent impurities showed depressions which were asymmetrical with respect to the peak and were interpreted by Caldwell and Klein in terms of scattering of thermal phonons by resonance modes associated with the impurities. A shell model was used to describe the phonons of the perfect lattice and a simple model of the impure lattice was assumed. This involved a change of mass at the defect site together with changes of the nearest-neighbor central force constant and was moderately successful in predicting the shape of the thermal-conductivity curves.

The shell-model phonons of Caldwell and Klein have also been used in calculations of the far-infrared absorption of monovalent impurities in sodium chloride, and for chemical impurities the experimental data could be fitted fairly well after adjusting force-constant changes.[1,10] In the case of bromine the main features of the experimental curve were reproduced by the nearest-neighbor central-force model, but for silver and fluorine more realistic models were required. For all these impurities the calculated peaks in the region of the acoustic-phonon critical points were about 6% too low, suggesting that the shell-model parameters used probably gave incorrect phonon frequencies. Further confirmation of this was provided by measurements of the band-mode absorption due to the natural isotopes of chlorine in sodium chloride,[2] for which the peaks in the calculated curve were approximately 4% too low. The isotope calculation does not involve force-constant changes and so provides a direct test of the shell-model parameters.

In this paper we present the results of an experimental and theoretical study of the far-infrared absorption spectra of a number of monovalent impurities in sodium chloride. Measurements have been made from 33 cm^{-1}

* Work supported in part by the Advanced Research Projects Agency under Contract No. SD-131.
† Present address: Clarendon Laboratory, Parks Road, Oxford, England.
[1] H. F. Macdonald and M. V. Klein, in *Proceedings of the International Conference on Localized Excitations in Solids, University of California, Irvine, California, 1967*, edited by R. F. Wallis (Plenum Press, Inc., New York, 1968).
[2] M. V. Klein and H. F. Macdonald, Phys. Rev. Letters **20**, 1031 (1968).
[3] See contributions by A. A. Maradudin, and A. J. Sievers, in *Proceedings of the International Conference on Localized Excitations in Solids, University of California, Irvine, California, 1967*, edited by by R. F. Wallis (Plenum Press, Inc., New York, 1968), and references therein.
[4] See Ref. 3 and, in addition, contributions by W. Hayes and B. Fritz, in *Proceedings of the International Conference on Localized Excitations in Solids, University of California, Irvine, California, 1967*, edited by R. F. Wallis (Plenum Press, Inc., New York, 1968).
[5] R. Weber, Phys. Letters **12**, 311 (1964).
[6] R. Weber and P. Nette, Phys. Letters **20**, 493 (1966).
[7] D. R. Bosomworth, Solid State Commun. **5**, 681 (1967).
[8] R. F. Caldwell and M. V. Klein, Phys. Rev. **158**, 851 (1967).
[9] C. K. Chau, M. V. Klein, and B. Wedding, Phys. Rev. Letters **17**, 521 (1966).
[10] M. V. Klein, in *Physics of Color Centers*, edited by W. B. Fowler (Academic Press Inc., New York, 1968).

to within a few wave numbers of the Reststrahlen frequency (174 cm^{-1} at liquid-helium temperature[11]). The aim of this work is to investigate to what extent simple defect models can explain the data over this relatively broad frequency range. Previous investigations have tended to concentrate only on the low-frequency resonance modes associated with defects, through effects such as their temperature dependence[12] and behavior under externally applied perturbation.[13] Calculations of the continuous impurity-induced absorption in the band-mode region have been limited both in their number and in the degree of their success. Only for the case of U centers in potassium bromide and iodide[14] has good agreement between theory and experiment been obtained over a wide frequency range in the far infrared.

II. EXPERIMENTAL

A. Technique

Absorption measurements at liquid-nitrogen and liquid-helium temperatures in the range 33–170 cm^{-1} were made using a Beckman IR 11 spectrophotometer which was fitted with a beam condenser. Cleaved single crystals of chemically pure sodium chloride, and sodium chloride doped with silver, lithium, potassium, fluorine, bromine, and iodine were mounted in a cryostat which enabled them to be moved into or out of radiation beam while at low temperature. The crystals were cooled by helium-exchange gas which was in thermal contact with the liquid refrigerant, and their temperature was measured using a germanium-resistance thermometer.

The spectrophotometer was used in the single-beam mode and the transmittance T of the sample obtained directly as the ratio of the radiation intensity with the sample in the beam to that with the sample out of the beam. The absorption constant α, as a function of frequency, ω was determined using the relation

$$T=(1-R)^2\exp(-\alpha d)/[1-R^2\exp(-2\alpha d)].$$

Here d is the sample thickness, and R the reflectance given by

$$R=[(n-1)^2+k^2]/[(n+1)^2+k^2]\simeq(n-1)^2/(n+1)^2,$$

where n and k are the real and imaginary parts of the index of refraction. For our experiments $k\ll1$, and the approximate expression for R on the right above was used. The frequency dependence of n was taken into account using the relation[15]

$$n^2=\epsilon_\infty+(\epsilon_0-\epsilon_\infty)/(1-\omega^2/\omega_0^2),$$

where ϵ_∞ and ϵ_0 are the high- and low-frequency dielectric constants, respectively. The effects of the chemical impurities on the ϵ_∞ and ϵ_0 were neglected and the impurity-induced absorption obtained as the difference in absorption constant between the doped and pure crystals. In this procedure care was taken to insure that structure observed in the impurity-induced absorption was real, and not simply a reflection of variations in the background absorption subtracted off. This was achieved by using doping levels such that the impurity absorption at liquid-helium temperature was substantially greater than that of the undoped crystal.

All of the crystals studied were cleaved from the same boules used by Caldwell and Klein in their thermal conductivity measurements.[8] The crystals were grown in this laboratory from reagent grade material which was pretreated for 12 h by bubbling Cl_2 gas through the melt to remove hydroxyl and carbonate impurities.[16] Analysis of the undoped material by a mass spectrograph showed that the major remaining impurity was calcium in concentrations of a few parts per million. In preliminary measurements certain of the chemical-impurity spectra showed a nonlinear dependence on concentration, as determined from the analysis of the thermal conductivity samples.[8,16] In order to confirm that this was not a real effect, additional concentration measurements were made using the infrared samples, thus eliminating variations of concentration within the boules.

The silver concentrations were determined by measuring the ultraviolet-absorption bands at 2100 and 2170 Å on a Cary Model 15 spectrophotometer, and using the relation between absorption coefficient and concentration given by Worlock.[17] A weak band at 2280 Å, which became more pronounced with heavier doping, was also observed. The intensity of this band did not scale with that of the two main bands, thus it was probably due to the formation of aggregate silver centers.

Analysis of the potassium, fluorine, and bromine samples was performed by the analytical staff of the Materials Research Laboratory. The potassium concentrations were measured by flame spectroscopy, and for bromine a neutron activation technique was used. The fluorine concentrations were determined using a specific ion electrode method in which aqueous solutions prepared for the infrared samples were compared with solutions containing known concentrations of F^- ions. This method was capable of a precision of better than

[11] G. R. Wilkinson and C. Smart (unpublished).
[12] S. Takeno and A. J. Sievers, Phys. Rev. Letters **15**, 1020 (1965).
[13] I. G. Nolt and A. J. Sievers, Phys. Rev. Letters **16**, 1103 (1966).
[14] T. Timusk, E. J. Woll, and T. Gethins, in *Proceedings of the International Conference on Localized Excitations in Solids, University of California, Irvine, California, 1967*, edited by R. F. Wallis (Plenum Press, Inc., New York, 1968).
[15] M. Born and K. Huang, *Dynamical Theory of Crystal Lattices* (Clarendon Press, Oxford, England, 1954).
[16] R. F. Caldwell, Ph.D. dissertation, University of Illinois, 1966 (unpublished).
[17] J. M. Worlock, Ph.D. dissertation, Cornell University, 1962 (unpublished); Phys. Rev. **147**, 636 (1966).

3% and revealed detailed information on the distribution of fluorine within the crystals. For low doping levels the fluorine concentration was fairly uniform, but at concentrations of the order of a few tenths of a mole percent variations of up to a factor of 2 were found in samples cleaved from adjacent parts of the boule.

Impurity concentrations in the samples used for infrared and for thermal conductivity often differed significantly. In the preliminary report of this work[1] the fluorine and bromine concentrations determined from the thermal-conductivity samples[8,16] were used, and some of the quoted concentrations are in error (see Figs. 3 and 4 of Ref. 1).

The iodine concentrations were determined using the results of the chemical analysis described by Caldwell and Klein[8] together with optical measurements on the long-wavelength side of the strong ultraviolet absorption due to iodine at 1820 Å.[16] The ultraviolet absorption of thin slices cleaved from the infrared samples was compared with that of crystals taken from alongside the samples used in the original analysis on a Zeiss PQM II spectrophotometer. The neutron-activation method could not be employed for the analysis of iodine in the presence of chlorine since the radioactive isotopes of these two elements have similar half-lives.

B. Results

In the remaining paragraphs of this section the main features of the absorption spectra due to six chemical impurities in sodium chloride will be described. Qualitative aspects of the results are discussed in relation to the thermal-conductivity measurements of Caldwell and Klein, a detailed comparison with theoretical calculations being postponed until Sec. V.

The main features of the absorption spectrum due to *silver* in sodium chloride are essentially independent of temperature and concentration, apart from a slight increase in the absorption near 140 cm^{-1} with increasing temperature (see Fig. 1 of Ref. 1). In this region the background absorption of the pure crystal is rising rapidly at nitrogen temperature and the observed increase is just within the limit of experimental error.

The resonance mode responsible for the thermal conductivity depression at about 35–50°K occurs at 53 cm^{-1} at 7°K and 52 cm^{-1} at 80°K, as found previously by Weber.[5] In the same temperature range its width increases from 12 to 14 cm^{-1}. In addition to this peak there is a broad absorption towards higher energy which shows distinctive structure in the region of the acoustic-phonon critical points of pure sodium chloride. This consists of a weak peak at 120.5 cm^{-1} and a strong one at 131 cm^{-1}, together with a shoulder at 155 cm^{-1} (see Fig. 8).

The *lithium* absorption in sodium chloride is shown in Fig. 1, in which the low-energy portion of the spectrum has been multiplied by 10. This system shows

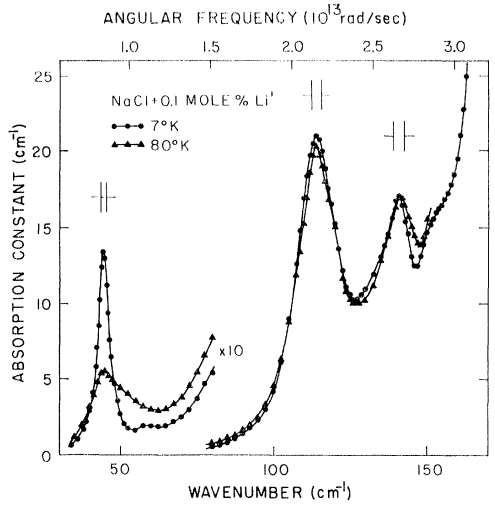

FIG. 1. Temperature dependence of the absorption of NaCl:Li^+.

a resonance-mode peak at 44.5 cm^{-1} with a half-width of 5 cm^{-1} at 7°K, and was first measured by Sievers.[18] On warming to 80°K the peak position and intensity of the resonance-mode absorption remain unchanged but its width increases to about 17 cm^{-1}. Accompanying the resonance mode there is again broad absorption towards higher energy with strong peaks at 114 and 141 cm^{-1}, and weak shoulder at about 154 cm^{-1}. Unlike the resonance-mode absorption this has no significant temperature dependence. The thermal-conductivity curves for lithium showed a broad depression, centered at about 40°K, which was almost three times weaker than that of the silver impurity. This result is consistent with the relative intensities of

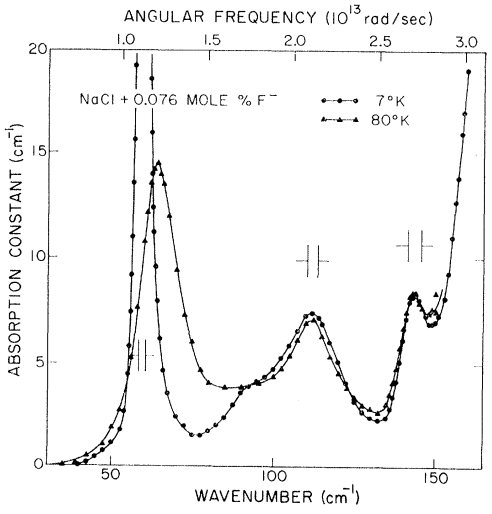

FIG. 2. Temperature dependence of the absorption of NaCl:F^-.

[18] S. Takeno, in *Proceedings of the International Conference on Localized Excitations in Solids, University of California, Irvine, California, 1967*, edited by R. F. Wallis (Plenum Press, Inc., New York, 1968).

the resonance-mode peaks associated with these two impurities, the integrated intensity of the silver peak being close to four times greater than that of lithium.

In contrast with silver and lithium, the *potassium* impurity shows no resonance-mode peak (see Fig. 9). This result is consistent with the thermal-conductivity measurements in which the observed depression, centered at 60°K, was very broad and almost an order of magnitude weaker than that for silver. However, the spectrum does show broad temperature-independent absorption in the region of the acoustic-phonon critical points. A weak peak occurs at 87 cm^{-1}, together with two stronger peaks at 122 and 143 cm^{-1}. The energies at these peaks are close to those of the TA(X), TA(L), and LA(X) phonons in pure sodium chloride which are 86.5, 122, and 142 cm^{-1}, respectively (see Sec. III). This, coupled with the lack of temperature dependence of the absorption between 7 and 80°K, indicates that we are observing single-phonon defect-activated band-mode absorption.

For the *fluorine* impurity the thermal-conductivity curves showed a strong depression below 15°K, with a much weaker depression near 40°K. This suggests that resonance-mode absorption might occur near 10 cm^{-1}, but this has not been found experimentally.[19] However, a resonance mode corresponding to the 40°K depression is observed at 59.5 cm^{-1} at 7°K (see Figs. 2 and 11). This band was first measured by Sievers,[19] and in our experiments has a resolution-limited width of 2 cm^{-1} at liquid-helium temperature. On warming to 80°K its peak position shifts to 64 cm^{-1}, while its width increases to 14 cm^{-1} and is comparable with that of the silver resonance. Since the peak absorption constant of the fluorine resonance at liquid-nitrogen temperature is an order of magnitude greater than that for silver, one might expect the 40°K depression of the fluorine thermal conductivity to be significantly greater than that for silver. Experimentally, the fractional depressions at 40°K for 0.1 mole% impurity concentration were almost identical. Qualitatively this can be understood from the higher density of phonon states at the fluorine resonance-mode frequency. This will make three-phonon scattering processes relatively more important than resonance-mode scattering and result in a weakening of the thermal-conductivity depression.

In addition to the fluorine resonance mode there is again absorption towards higher energy, with a broad peak at 112 cm^{-1} and a narrow one at 144 cm^{-1}. As was the case for the lithium impurity, these features remain unchanged on warming from 7 to 80°K, as shown in Fig. 2. Additional weak temperature-dependent peaks have been observed in the vicinity of the resonance mode in heavily doped crystals[1] and are probably due to pairs of fluorine ions. These peaks have not been studied in depth.

[19] A. J. Sievers (private communication).

The main features of the absorption spectra of *bromine* and *iodine* (also potassium) in sodium chloride are all very similar (see Figs. 12 and 13, also Fig. 9). This is reflected in the thermal-conductivity curves of these three impurities, which showed fractional depressions of 15–20% in the range 50–60°K for defect concentrations of 0.1 mole%. The bromine absorption consists of two weak peaks at 85 and 117 cm^{-1}, with a stronger one at 140 cm^{-1}. For iodine similar peaks occur at 71, 120, and 140 cm^{-1}. Both absorption curves are essentially temperature-independent and the peak energies are close to those of the phonon critical points compared earlier with the potassium results.

The far-infrared absorption due to the natural isotopes of chlorine will be described in Sec. III. There, the experimental result is used to determine input parameters for a shell-model calculation of the phonon spectrum of sodium chloride. This calculation will then be used in Sec. V to interpret the chemical impurity-induced absorption described above.

III. SHELL-MODEL CALCULATION

In order to calculate the optical absorption due to monovalent impurities in sodium chloride a detailed knowledge of the frequencies and polarization vectors of the phonons of the pure crystal is necessary. We have obtained this information using a shell model of the same form as that employed by Caldwell and Klein in the analysis at their thermal-conductivity experiments. The model is similar to those used successfully at Chalk River to fit neutron-determined dispersion curves for potassium bromide and sodium iodide,[20–22] potassium iodide,[23] and, more recently, lithium fluoride.[24] In the absence of neutron-determined dispersion curves for sodium chloride,[25] Caldwell and Klein evaluated the parameters for their shell-model calculation from elastic constants and dielectric data previously used by Karo and Hardy[26] in a "deformation dipole" model calculation for sodium chloride.

A major disadvantage of the thermal-conductivity calculation is that it involves averages over all phonons and is thus insensitive to the detailed properties of the phonon spectrum. In addition, assumptions concerning the processes governing the scattering of thermal phonons have to be made. In contrast the calculation of the isotope-induced band-mode absorption depends

[20] A. D. B. Woods, W. Cochran, and B. N. Brockhouse, Phys. Rev. **119**, 980 (1960).
[21] A. D. B. Woods, B. N. Brockhouse, R. A. Cowley, and W. Cocharan, Phys. Rev. **131**, 1025 (1963).
[22] R. A. Cowley, W. Cochran, B. N. Brockhouse, and A. D. B. Woods, Phys. Rev. **131**, 1030 (1963).
[23] G. Dolling, R. A. Cowley, C. Schittenhelm, and I. M. Thorsen, Phys. Rev. **147**, 577 (1966).
[24] G. Dolling, H. G. Smith, R. M. Nicklow, P. R. Vijayaraghaven, and M. K. Wilkinson, Bull. Am. Phys. Soc. **12**, 557 (1967); Phys. Rev. **168**, 970 (1968).
[25] Neutron-determined dispersion curves for sodium chloride have recently been obtained at room temperature by R. E. Schmunk (private communication).
[26] A. M. Karo and J. R. Hardy, Phys. Rev. **141**, A696 (1966).

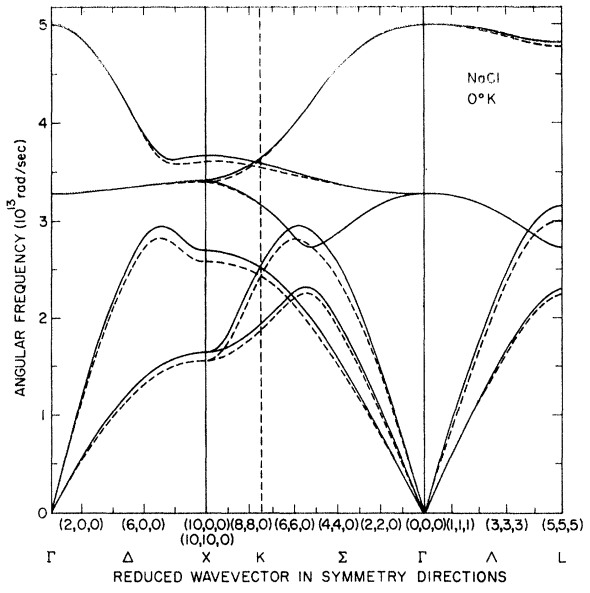

FIG. 3. Effect of variation of elastic constants on the dispersion curves for NaCl. Reduced wave vector in units of $10\pi/r_0$. (Full curve from present calculation, dashed curve from Caldwell and Klein's calculation.)

only on the parameters on the particular shell model used (see Sec. IV), and thus provides a more sensitive test of these parameters. From a comparison of the experimental absorption due to the natural isotopes of chlorine in sodium chloride with a calculation using the phonons of Caldwell and Klein, we have concluded that these phonons have too little energy in the acoustic branches.[2] We have therefore recalculated the phonon frequencies and polarization vectors for sodium chloride using the isotope data to adjust the shell-model parameters.

A detailed description of the shell model used in this calculation has already been given,[8,16] so only a brief summary of its main features will be presented here. The model involves nine parameters[20,22]: A, B'', A', B', Z, α_+, α_-, d_+, d_-. These describe the short-range nearest-neighbor and second-nearest-neighbor negative-ion interactions, the ionic charge, and the electronic and short-range polarizabilities of the positive and negative ions, respectively. The nine parameters are related to measureable constants by only five equations, and in order to reduce the number of undetermined parameters we have followed Caldwell and Klein in making the following assumptions: (a) The electronic polarizabilities are equal to the ionic polarizabilities, (b) the ionic charge $Z=1$, and (c) the force between next-nearest-neighbor negative ions is a van der Waals force, which gives $A'=-7B'$. The remaining five parameters are then determined from the relations obtained from the Appendix of Ref. 20:

$$C_{11}=(e^2/r_0v)[-2.555Z^2+\tfrac{1}{2}(A+A'+B')], \quad (1a)$$

$$C_{12}=(e^2/r_0v)(0.696Z^2-\tfrac{1}{4}B'+\tfrac{1}{4}A'-\tfrac{1}{2}B''), \quad (1b)$$

$$C_{44}=(e^2/r_0v)(0.696Z^2-\tfrac{1}{4}B'+\tfrac{1}{4}A'+\tfrac{1}{2}B''), \quad (1c)$$

$$\epsilon_0-\epsilon_\infty=4\pi(\epsilon_\infty+2)^2(Z+d_+-d_-)e^2/9v\mu\omega_0^2, \quad (1d)$$

$$R_0=e^2[d_+^2/\alpha_++d_-^2/\alpha_-]+\mu\omega_0^2[(\epsilon_0+2)/(\epsilon_\infty+2)]. \quad (1e)$$

The first three equations involve the elastic constants and the last two are the generalized Szigeti relations. r_0 is the nearest-neighbor distance, $v=2r_0^3$ is the volume of the unit cell, and μ its reduced mass.

Preliminary calculations of the phonon energies for a small number of points in k space, along symmetry directions and around the edge of the first Brillouin zone, were performed in order to determine the effects of variations of the shell-model parameters. It was found that, in general, the elastic constants determined the acoustic phonon energies, through Eqs. (1a)–(1c), while those of the optical phonons were influenced more by the dielectric data, through Eqs. (1d) and (1e). For example, changing the value of the ionic charge produced only small variations in the acoustic phonon energies, while the optical phonons were considerably modified, particularly the LO branch towards the edge of the zone. However, varying the values of the elastic constants significantly altered the acoustic phonon energies, but had little or no effect on the optical phonons. This is illustrated in Fig. 3, where dispersion curves for the three principal crystal directions obtained in the present calculation are compared with those of Caldwell and Klein. The parameters used in the two calculations are given in Table I, and differ only in the values of the three elastic constants.

Since the isotope data which we were using to adjust the shell-model parameters related to acoustic phonons, it was decided to utilize the above property and vary

TABLE I. Summary of input data for shell-model calculations.

Elastic constants (10^{12} dyn/cm^2)	$C_{11}=0.6300$[a]	$C_{12}=0.1354$[a]	$C_{44}=0.1454$[a]
	$C_{11}=0.5750$[b]	$C_{12}=0.0986$[b]	$C_{44}=0.1327$[b]
	$C_{11}=0.5733$[c]	$C_{12}=0.1123$[c]	$C_{44}=0.1331$[c]
Dielectric constants	$\epsilon_0=5.45$	$\epsilon_\infty=2.349$	
Ionic polarizabilities (10^{-24} cm^3)	$\alpha_+=0.255$	$\alpha_-=2.974$	
Reststrahlen frequency (10^{13} sec^{-1})	$\omega_0=3.277$		
Lattice constant (10^{-8} cm)	$r_0=2.7935$		

[a] Values used in present calculation.
[b] Values used by Caldwell and Klein.
[c] Values obtained from ultrasonic measurements at 4.2°K (Ref. 28).

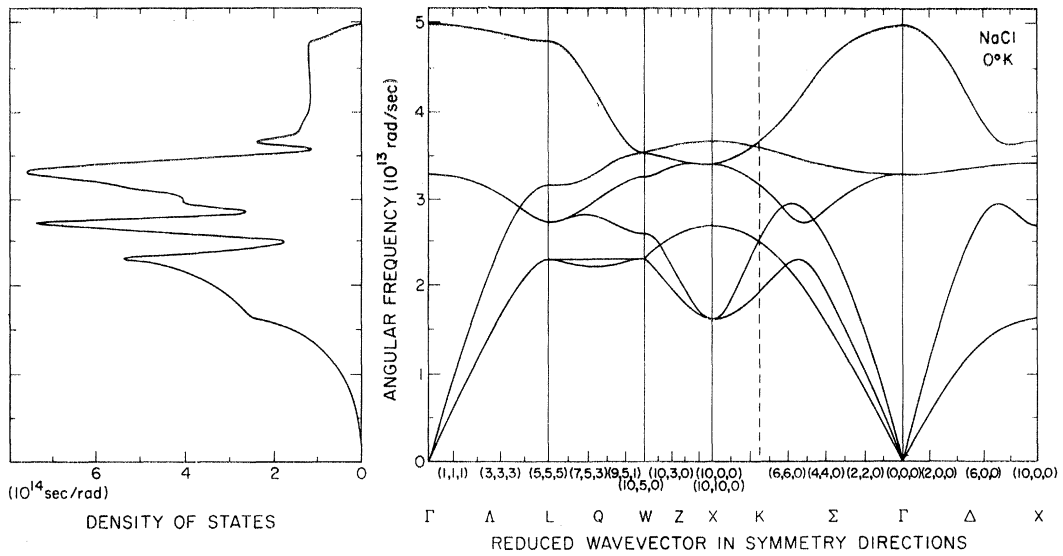

FIG. 4. Calculated dispersion curves and smoothed density-of-states histogram for NaCl. Reduced wave vector in units of $10\pi/r_0$, and density-of-states curve normalized to unity.

the acoustic-phonon energies by changing the values of the elastic constants used in the shell-model calculation. From the preliminary calculations for a small number of points in k space, an appropriate combination of elastic constants was selected. The phonon frequencies and polarization vectors were then evaluated for k vectors in 1/48 of the Brillouin zone, and their values for a total of 64 000 points in the full zone generated by the application of symmetry operations.[27] Density-of-states histograms were computed for a total of 384 000 points using the bin-staggering technique described by Caldwell and Klein. This gave an effective bin width of 1.18 cm^{-1}, which is comparable with the spectral resolution in the experimental measurements. The results of the shell-model calculation, in the form of dispersion curves for various directions in k space and the full density of states for sodium chloride obtained by drawing a smooth curve through the histogram, are shown in Fig. 4.

The isotope-induced absorption, calculated using the present phonons and also the phonons of Caldwell and Klein, is compared with the experimental result in Fig. 5. As expected from the procedure used to adjust the shell-model parameters, the energies of the two peaks in the curve calculated using the new phonons are in good agreement with experiment. In addition the intensity agreement, particularly towards higher energy, is considerably improved over that obtained with the Caldwell and Klein phonons. The significance of this will be discussed later in Sec. V A.

The values of the elastic constants of sodium chloride used in the present calculation may be compared with experimental values at 4.2°K obtained using an ultrasonic pulse technique,[28] which are also given in Table I. The experimental values of C_{11} and C_{44} are about 10% lower, and that of C_{12} about 20% lower, than the values used here. These discrepancies are outside the limits of experimental error, which were 1% for C_{11} and C_{44} and 4% for C_{12}. For lithium fluoride at room temperature similar differences exist between ultrasonically measured elastic constants and those obtained, using Eqs. (1a)–(1c), from a shell-model fit to neutron-determined dispersion curves.[24] In this case, the measured value of C_{11} is 11% lower than the shell-model value, while the mean of the measured values of C_{12} and C_{44} (which

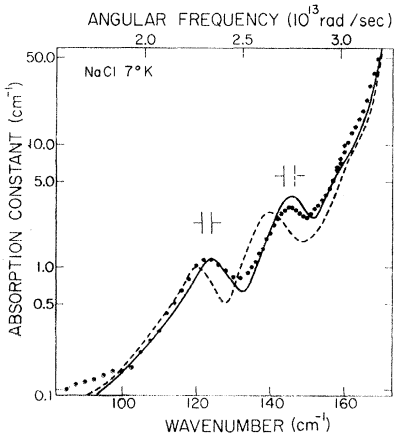

FIG. 5. Band-mode absorption at 7°K due to the natural isotopes in NaCl, 75.4% Cl^{35} and 24.6% Cl^{37}. (Full curve, present calculation; dashed curve, calculated using the phonons of Caldwell and Klein.)

[27] T. Timusk and M. V. Klein, Phys. Rev. 141, 664 (1966).

[28] J. T. Lewis, A. Lehoczky, and C. V. Briscoe, Bull. Am. Phys. Soc. 10, 44 (1965).

were assumed equal in the shell-model calculation) is 6% less than the shell-model value. In other alkali halides good agreement has been found between ultrasonic and shell-model elastic constants. In the case of potassium iodide the two sets of values agree to better than 3%,[23] and, in addition, Brillouin scattering measurements[29] on this crystal (also potassium and rubidium chlorides) yield elastic constants within a few percent of the ultrasonic values.

The failure of the present shell model to reproduce the correct elastic constants for sodium chloride, while giving a good description of the acoustic phonons as demonstrated by the isotope results, may arise from its comparative simplicity. A recent calculation by Nusslein and Schröder[30] using a "breathing" shell model and the ultrasonically measured elastic constants gave acoustic-phonon energies within a few percent of those obtained in the present calculation. This suggests that this form of the shell model might be more appropriate for sodium chloride. Another factor which may be important is the neglect of anharmonic effects in the shell-model description of the perfect lattice. These will be more significant in the lighter alkali halides where the zero-point displacements of the ions may be relatively large.

IV. OPTICAL ABSORPTION AND DEFECT MODELS

The calculation of the optical absorption due to monovalent impurities in an alkali halide lattice employing a nearest-neighbor central force model has been described in detail by Klein.[10] Similar calculations have been performed by Benedek and Nardelli.[31] In Sec. IV A an outline of the main features of the derivation of the impurity-induced absorption constant will be given for the limiting cases of a weakly perturbing and a strongly perturbing defect. In Sec. IV B simple extensions of the nearest-neighbor central-force model, aimed at giving a more realistic description of the imperfect crystal, will be described.

A. Absorption-Constant Calculation

For a harmonic crystal containing substitutional monovalent impurities, the dielectric constant at angular frequency ω may be written[2,32] as

$$\epsilon(\omega)=n_\infty{}^2+(4\pi e_t{}^{*2}/v\mu)(0,\mathrm{TO}|\langle G(\omega^2-i0^+)\rangle|0,\mathrm{TO}). \quad (2)$$

Here n_∞ is the high-frequency refractive index, $e_t{}^*$ the macroscopic effective charge associated with the $k=0$, TO phonon, v the volume of a unit cell, $G(z)=(A-zI)^{-1}$ the Green's function matrix of the entire imperfect crystal, and $|0,\mathrm{TO})$ a normalized eigenvector of the $k=0$, TO phonon. A is the dynamic matrix and $\langle\cdots\rangle$ denotes a configurational average over impurity sites. G is given in terms of the Green's function matrix for the perfect crystal, $G_0=(A_0-zI)^{-1}$, and the perturbation matrix Γ by the expression,

$$G=G_0I/(I+\Gamma G_0)\simeq G_0-G_0\Gamma G_0+G_0\Gamma G_0\Gamma G_0\cdots. \quad (3)$$

For a weak perturbation Γ, such as that due to an isotopic defect, the expansion of Eq. (3) should converge rapidly. In the isotope calculation we assume a virtual crystal model in which the unperturbed phonons diagonalize the dynamical matrix $A_0=\langle A\rangle$. Then, since $\Gamma=A-A_0$, we have $\langle\Gamma\rangle=0$, and to the lowest order

$$\langle G\rangle=G_0+G_0\langle\Gamma G_0\Gamma\rangle G_0. \quad (4)$$

In the present experiment only the chlorine sublattice carries more than one isotope, and Γ is a sum of terms over this sublattice of the form

$$\Gamma(L,L')=-\sum_L \Delta M_-(L)\omega^2\delta(L,L')/M_-,$$

where M_- is the mean chlorine-ion mass, $\delta(L,L')$ the Kronecker δ, and ΔM_- the deviation at site L of the true mass from M_-. One can then show that

$$(0,\mathrm{TO}|\langle\Gamma G_0\Gamma\rangle|0,\mathrm{TO}\rangle = (\mu/M_-)G_{--}\langle(\Delta M_-\omega^2/M_-)^2\rangle, \quad (5)$$

where G_{--} is the diagonal matrix element of G_0 at the chlorine-ion site.

When Eqs. (3)–(5) are substituted into Eq. (2), and the relation $G_0(z)|0,\mathrm{TO})=(\omega_0{}^2-z)^{-1}|0,\mathrm{TO})$ is used, the result for the isotope-induced absorption constant becomes

$$\alpha(\omega)=\frac{e_t{}^{*2}}{n(\omega)cM_-{}^3v}\frac{2\pi^2\omega^4\rho^-(\omega)}{(\omega_0{}^2-\omega^2)^2}\langle(\Delta M_-)^2\rangle. \quad (6)$$

Here, c is the velocity of light, $n(\omega)$ the refractive index at frequency ω, and $\rho^-(\omega)$ the phonon density of states for the chlorine sublattice given by

$$\rho^-(\omega)=\sum_{k\lambda}|\epsilon^-(k\lambda)|^2\delta(\omega_{k\lambda}-\omega)/\sum_{k\lambda}|\epsilon^-(k\lambda)|^2,$$

where $\epsilon^-(k\lambda)$ is the chlorine-ion–polarization vector for a mode of wave vector k and branch index λ. The normalization for $\rho^-(\omega)$ is

$$\int_0^\infty \rho^-(\omega)d\omega=1.$$

The above derivation of the isotope-induced absorption is valid for the limit of a weakly perturbing, high-concentration defect. For the chemical impurity-induced absorption the calculation is carried out in the limit of a strongly perturbing, low-concentration defect. The two approaches are similar, but there are

[29] G. B. Benedek and K. Fritsch, Phys. Rev. **149**, 647 (1966).
[30] V. Nusslein and U. Schröder, Phys. Status Solidi **21**, 309 (1967).
[31] G. Benedek and G. F. Nardelli, Phys. Rev. **155**, 1004 (1967).
[32] E. Burstein, in *Proceedings of the International Conference on Lattice Dynamics, Copenhagen, Denmark, 1963*, edited by R. F. Wallis (Pergamon Press, Oxford, England, 1965).

important differences. First, the expansion of Eq. (3) no longer converges well for a strong perturbation Γ, and G must be expressed in the form

$$G=G_0-G_0\Gamma G_0+G_0\Gamma G_0\Gamma G_0-\cdots$$
$$=G_0-G_0TG_0, \quad (7)$$

where

$$T=\Gamma[I/(I+G_0\Gamma)]. \quad (8)$$

This is the T matrix for the entire impure crystal and involves the inversion of extremely large matrices, defined in a $3r\eta$-dimensional space (for a crystal with r atoms per unit cell and η unit cells). The calculation of the impurity-induced absorption is made tractable by the fact that this inversion need be performed only within a relatively small vector space, the "space of Γ," containing the nonzero elements of Γ. Further simplifications result from the use of symmetry arguments. If the vectors defining Γ are chosen such that they transform like irreducible representations of the point group of the sodium or chlorine-ion sites (octahedral O_h), it can be shown that for the absorption calculation the space of Γ reduces to that spanned by the odd-parity vectors of T_{1u} symmetry. Detailed discussions of the properties of the T matrix and its use in the calculation of absorption constants can be found in two papers by Klein.[10,33]

A second difference between the isotopic and chemical impurity calculations comes in the treatment of the configurational average appearing in Eq. (2). For the chemical impurity this is replaced by the product of the absorption constant calculated for a single isolated impurity and the total number of impurities. This approximation is good when the perturbation matrix is sufficiently localized and when there is a dilute random distribution of impurities. After substitution of Eq. (8) into Eq. (2) and some manipulation, the result for the chemical impurity-induced absorption constant is given by

$$\alpha(\omega)=\frac{4\pi N}{n(\omega)c}\frac{\omega}{(\omega_0^2-\omega^2)^2}\frac{e_i^{*2}\mathfrak{N}}{\mu}$$
$$\times\mathfrak{Im}(0,\mathrm{TO}|t(\omega^2-i0^+)|0,\mathrm{TO}). \quad (9)$$

Here N is the defect concentration per unit volume, $\mathfrak{N}$ is the total number of unit cells, and $t(z)$ is that part of the T matrix within the space of Γ.

In calculating the impurity-induced absorption from Eqs. (6) and (9), we shall follow the suggestion of Szigeti[32,34] and set

$$e_i^*=\tfrac{1}{3}e^*(n_\infty^2+2),$$

where e^* is the Szigeti effective charge. This takes into account the contribution to the polarization of the crystal from the electron distribution, as well as that due to the ionic motion [see Eq. (7–57) of Ref. 10].

Equations (5) and (9) show that the radiation couples directly to a vibrational configuration which consists of a $k=0$, TO phonon. The resulting frequency spectrum is no longer the δ function at $\omega=\omega_0$ which is obtained for the pure crystal via the G_0 terms in Eqs. (4) and (7); it now has the additional continuous spectrum given by Eqs. (6) and (9). Caldwell and Klein showed that the resonance modes responsible for pronounced thermal-conductivity depressions consist primarily of a relative motion of the defect and two of its nearest neighbors along a line joining them. In this motion, which has the same T_{1u} symmetry as the $k=0$, TO phonon, the defect displacement may be large compared with that of the atom which it replaces and can thus couple strongly to infrared radiation. In addition, motion of the host atoms at higher band-mode frequencies may involve relative displacements of the defect and its nearest-neighbors which have T_{1u} symmetry. Here the displacements of the defect and its neighbors are of similar magnitude. It is this type of process which is responsible for the high-energy structure observed in the experimental spectra described in Sec. II B.

B. Defect Models

The isotope result of Eq. (6) shows that the induced absorption is proportional to the chlorine-ion density of states. This in turn is proportional to the imaginary part of the chlorine-ion Green's function, which is calculated directly from the eigenvectors obtained from the shell-model calculation. The expression for the absorption constant thus depends only on the shell-model parameters, and represents a consistent shell-model treatment of the imperfect crystal. This is achieved in a fairly simple manner because the chlorine isotopes are true weakly perturbing defects and may be adequately described by just a mass change at each defect site.

For the chemical impurities this situation no longer holds, and in general the force-constant changes, as well as the mass change, due to the defect must be considered. In the present calculations this is done through the Γ matrix and the T-matrix formalism. Since the usefulness of this method depends on the limitation of the size of the space of Γ (or equivalently the number of defect parameters), while a consistent shell-model description would tend towards extra parameters, we have chosen to compromise and use the shell-model results to evaluate the unperturbed Green's functions appearing in Eqs. (7) and (8), together with a point-ion model to evaluate Γ. This enables the force-constant change between the defect and, say, a nearest-neighbor ion to be characterized by a single parameter rather than the two which would be required for a shell-model description, i.e., defect core/defect shell, and defect shell/nearest-neighbor shell force-constant changes. We

[33] M. V. Klein, Phys. Rev. **141**, 716 (1966).
[34] B. Szigeti, Trans. Faraday Soc. **45**, 155 (1949).

feel that this approach provides a physically more reasonable and satisfactory picture of the perturbed crystal than that resulting from a consistent point-ion treatment. In addition it is particularly useful in extending the nearest-neighbor central-force model to include effects of more distant neighbors, where a full shell-model description would involve a prohibitive number of force-constant parameters.

In fitting the experimental spectra described in Sec. II B, we have used five defect models, which are as follows:

(I) Nearest-neighbor central-force model. This is one of the simplest and most widely used defect models.[3,4] It involves a change of mass at the defect site, together with a change in the central-force constant coupling the defect to its six nearest neighbors.

(II) Noncentral-force model. In this model a change in the nearest-neighbor noncentral-force constant is added to model I.

(III) Next-nearest-neighbor central-force model. Here the central-force constant changes between the defect and both its six nearest neighbors and its 12 second-nearest neighbors, are included.

(IV) Lattice-relaxation model. This model takes account of changes in the force constants between the nearest and more distant neighbors of the defect, which may result from inward or outward relaxation of the nearest-neighbors when the size of the impurity differs appreciably from that of the atom which it replaces. It was first proposed by Gethins, Timusk, and Woll,[35] and includes changes in the nearest-neighbor central-force constant and in the central-force constant between the nearest neighbors and their nearest neighbors in the direction away from the defect (these are fourth-neighbors to the defect).

(V) Charge-defect model. This is the "deformation charge defect model" which has recently been described in detail by Martin.[36] It is an extension of model I in which the Szigeti effective charge of the defect is allowed to differ from that of its nearest neighbors. When the polarizability of a defect differs from that of the ion which it replaces, there will be a change in the effective charge of at least the defect and its nearest-neighbors. In models I–IV this effect is not included, and the value of e^* appearing in Eq. (10) is common to both the defect and its neighbors.

In deciding which force-constant changes might be important for a particular impurity it is convenient to refer to rigid-ion pictures of the defect and its immediate neighbors. These are shown for the six chemical impurities studied in Fig. 6, where the size of the circles

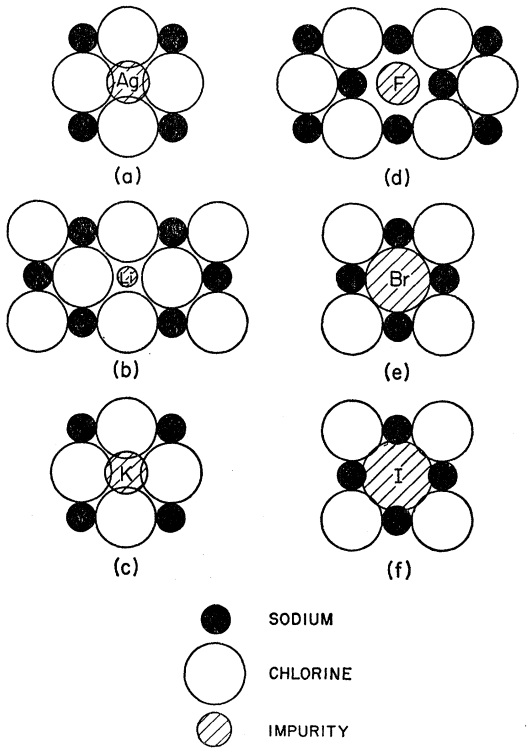

FIG. 6. Rigid-ion representations of the substitutional chemical impurities in NaCl.

representing the various ions are proportional to their ionic radii.[37]

Consider first the silver and potassium impurities in sodium chloride shown in Figs. 6(a) and 6(c). Although their ionic radii are, respectively, about 35 and 40% greater than that of the sodium ion which they replace, they are shielded from the second-neighbor sodiums by the large nearest-neighbor chlorine ions. This suggests that to a good approximation only the nearest-neighbor force constant will be changed and model I should be applicable. Also the electron distribution of a negative ion is less strongly bound to the central core than for a positive ion, as shown by the higher polarizabilities of negative ions in general.[38] Thus, the nearest-neighbor chlorines will tend to deform in order to accommodate the silver and potassium impurities rather than relax outwards, and the considerations of model IV will not be important. Section V will show that the above conclusions are partially correct, but that for silver it is necessary to include the effects of noncentral forces through model II (see, also, Ref. 1). In addition, the lattice constant of silver chloride is slightly less than that of sodium chloride, indicating that the effective size of the silver impurity is probably smaller than that shown in Fig.

[35] T. Gethins, T. Timusk, and E. J. Woll, Phys. Rev. **157**, 744 (1967).
[36] T. P. Martin, Phys. Rev. **170**, 779 (1968).
[37] V. M. Goldschmidt, Avhandl. Norske Videnskaps-Akad. Oslo, I. Mat. Naturv. Kl. **2**, 1 (1926).
[38] J. R. Tessmann, A. H. Kahn, and W. Schockley, Phys. Rev. **92**, 890 (1953).

6(a) and that the rigid-ion picture is inappropriate in this case.

The lithium impurity shown in Fig. 6(b), has an ionic radius approximately 35% less than that of sodium. Hence, one expects a reduction of the nearest-neighbor central-force constant and also some inward relaxation of the nearest neighbors, indicating that model IV might be appropriate.

For the substitutional impurities on the chlorine sublattice in sodium chloride the small nearest-neighbor sodium ions provide only partial shielding of the defect from the second-neighbor chlorines. For bromine and iodine, whose ionic radii are, respectively, 10 and 20% greater than that of chlorine, the rigid-ion pictures of Figs. 6(e) and 6(f) show the defect-electron distributions almost overlapping with those of the second-nearest neighbors. Outward movement of the nearest-neighbor sodium ions is expected to be small for these large deformable negative impurities; thus, model III should be applicable for bromine and iodine.

Finally, for the fluorine impurity, which is shown in Fig. 6(d) and has an ionic radius 25% less than that of chlorine, a reduction of the nearest-neighbor central-force constant is expected. This may be offset to some extent by an inward relaxation of the nearest-neighbor sodium ions, which will lead in turn to a reduction of the nearest-neighbor/fourth-neighbor force constant. In Sec. V we use model IV to show that this situation appears to apply to the fluorine impurity in sodium chloride.

Although the above arguments are highly qualitative, they are included because many of the ideas which have proved valuable in understanding the chemical-impurity spectra originated from rigid-ion pictures of the imperfect lattice of the type shown in Fig. 6.

V. RESULTS AND DISCUSSION

A. Isotopic Impurities

For the special case of an isotopic impurity the result of Eq. (6) shows that the induced absorption in the band-mode region is proportional to the density of states of the sublattice carrying the defect, and to a smoothly varying frequency factor, $\omega^4/(\omega_0^2-\omega^2)^2$. It is thus possible to identify peaks in the density of states with structure in the experimental curve. However, because of the complex behavior of the dispersion curves of sodium chloride in the region of the acoustic phonon critical points (see Fig. 4), it is difficult to assign peaks in the chlorine isotope-induced absorption shown in Fig. 5 to specific van Hove singularities. The 123-cm^{-1} peak is probably due to TA phonons from the L and W symmetry points, and from points near the edge of the zone along the Q direction joining them. The 145.5-cm^{-1} peak appears to be associated principally with phonons from the LA(X) critical-point region. These assignments are consistent with selection rules derived by Loudon[39] for one-phonon absorption activated by isotopic defects in the sodium-chloride lattice. The 86.5-cm^{-1} density-of-states feature associated with the TA(X) critical point was not detected in the isotope measurements due to lack of sensitivity of the IR 11 spectrophotometer. This was expected to occur as a slight change of slope, rather than a well-defined absorption peak.

In Sec. III we noted the good intensity agreement between the experimental and calculated isotope-induced absorption curves for sodium chloride. In the theoretical curves the only parameter not determined by the shell-model calculation is the Szigeti effective charge of Eq. (10) and for the curves shown in Fig. 5, we have used the value for sodium chloride, $e^*/e=0.74$,[40] where e is the electronic charge. Since the deviation of e^*/e from unity results from the polarizability of the sodium and chlorine ions, the use of this value is compatible with a consistent shell-model treatment of the isotope-induced absorption. In addition similar intensity agreement has been obtained in a calculation of the absorption due to lithium isotopes in lithium fluoride,[1,41] so that the good agreement in the present case is probably more than fortuitous. In Sec. V B it will be found that for the chemical impurities, for which a point-ion model is used to evaluate the Γ matrix, it is necessary to assume values of e^*/e different from the sodium-chloride value given above in order to obtain reasonable intensity agreement.

B. Chemical Impurities

In this section the experimental results of Sec. II B will be compared with calculations based on the theory of Secs. III and IV. We begin with a few general remarks, and then consider the six chemical impurities individually.

The result of Eq. (9) shows that the chemical impurity-induced absorption no longer has a simple dependence on the density of states of the host crystal, as was the case for the weakly perturbing isotopic defect discussed above. Instead, the absorption may be considered to be proportional to a modified or perturbed density of states, with the extent of this modification being determined by the magnitude of the mass and force-constant changes introduced through the Γ matrix. For moderately perturbing defects, such as potassium and bromine, the main features of the density of states may still be recognized in the absorption curve. The three peaks in the experimental spectra of these impurities occur close to peaks in the unperturbed density of states at 86.5, 122, and 144 cm^{-1} (see Fig. 4). The main effect of the Γ matrix is to change the relative intensities of the various peaks, as can be observed by comparing the isotope result of Fig. 5 with the potas-

[39] R. Loudon, Proc. Phys. Soc. (London) 84, 379 (1964).
[40] D. H. Martin, Advan. Phys. 14, 39 (1965).
[41] M. V. Klein and H. F. Macdonald (to be published).

sium and bromine impurity results shown in Figs. 9 and 12, respectively.

In the case of strongly perturbing defects, where the mass and/or force-constant changes are relatively large, the absorption curve may contain strong peaks which have no obvious correspondence with the unperturbed density of states. The silver, lithium, and fluorine impurities in sodium chloride all show well-defined resonance-mode peaks in regions where the density of states is low and displays no structure. In addition, for silver a strong peak is observed at 131 cm^{-1}, where the unperturbed density of states has a minimum, while for lithium and fluorine broad peaks occur at 114 and 112 cm^{-1}, respectively, approximately 10 cm^{-1} lower in energy than the nearest density-of-states maximum.

The iodine impurity in sodium chloride appears to be intermediate between the moderately and strongly perturbing defect cases just described. The lowest energy maximum in the experimental curve (see Fig. 13) occurs approximately 15 cm^{-1} below the first acoustic phonon critical point at TA(X), and thus cannot be properly described as a defect-activated band-mode absorption peak. Instead it may be considered as a limiting case of a resonance-mode absorption of the type found for silver, lithium, and fluorine (also copper[6]) and its increased width, compared with that of these resonances, can be explained by its proximity to the broad band-mode absorption towards higher energy.

The above considerations reveal the importance of having an accurate model for the phonons of the host crystal when attempting to fit chemical impurity-induced absorption data. To a limited degree, force-constant changes may compensate for errors in the phonon energies, but in the present work the isotope results indicate that the latter have been minimized. In addition, force-constant changes which appeared physically unreasonable have been avoided. In fitting the experimental data for the six chemical impurities studied we have used up to two force constants as adjustable parameters, together with the appropriate change of mass at the defect site. The values of these force constants were determined first by the criterion that the calculated absorption should reproduce the main qualitative features of the experimental curves, namely, the shape and relative intensities of the various peaks. Less emphasis was placed on reproducing the absolute intensity of the experimental absorption and, with the exception of the lithium and potassium impurities, this was achieved by treating the Szigeti effective charge of Eq. (10) as an additional adjustable parameter.

In models I–IV the Szigeti effective charge appears in the expression for the absorption constant as a frequency-independent multiplying factor [see Eqs. (9) and (10)], and thus raises or lowers the whole theoretical curve without altering its shape. In model V it is expressed as a tensor and results in additional terms in the expression for the impurity-induced absorption [see Eq. (11) of Ref. 36]. These give rise to changes in the shape of the theoretical curve, when the defect effective charge is different from that of the host ions, and these will be illustrated below in connection with the potassium and iodine impurity data.

In the following paragraphs we describe in detail a comparison of theoretical calculations with the experimental results for each impurity. The extent to which the various defect models of Sec. IV B are able to account for the observed far-infrared spectra is also discussed.

1. Silver

The calculated absorption spectra due to silver in sodium chloride obtained using models I and II (with $e^*/e=1.0$) are compared in Fig. 7. For model I the nearest-neighbor central-force constant was adjusted to give the resonance-mode peak at the experimental position of 53 cm^{-1}, which required a decrease of approximately 50% in this force constant.[42] Although the shape of the resonance mode is given fairly well, its intensity is overestimated by a factor of almost 4 (see Fig. 8), and there is a minimum in the calculated curve near 131 cm^{-1}, where the experimental result

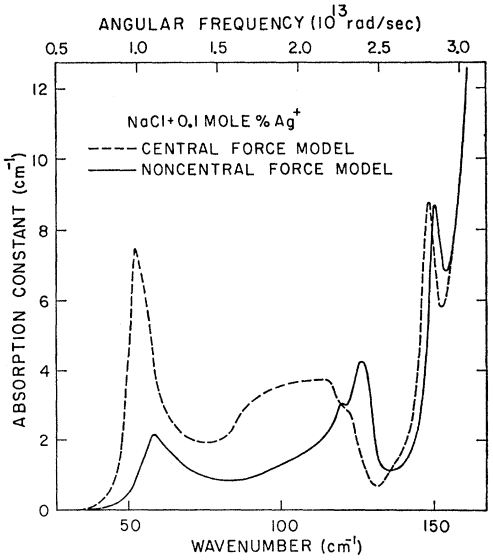

FIG. 7. Calculated absorption of NaCl:Ag^+, with $e^*/e=1.0$. (Full curve, model II with change in central force constant, 1000 erg/cm^2, and change in noncentral force constant, −1800 erg/cm^2; dashed curve, model I with change in central force constant, −8500 erg/cm^2.)

[42] Here the effective force constant for the unperturbed crystal is defined as the absolute value of the change in the nearest-neighbor central force constant required to produce a zero-frequency resonance in the T_{1u} symmetry vibrational configuration in which the defect and two of its nearest neighbors move along the line joining them without relative displacement. For a more complete discussion see Sec. IV D of Ref. 10.

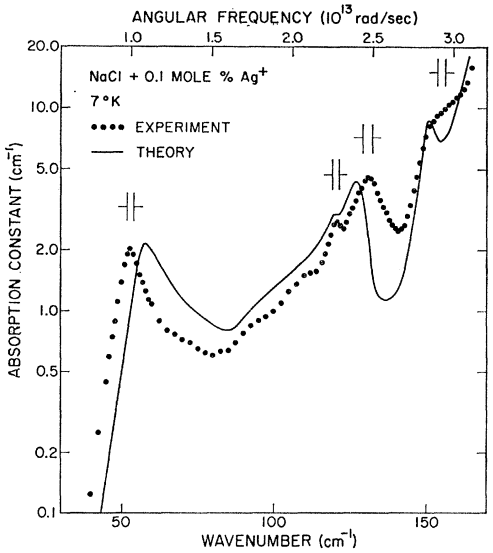

FIG. 8. Comparison of theory and experiment for NaCl:Ag^+, using model I with parameters as for full curve of Fig. 7.

shows a strong maximum. Thus, the nearest-neighbor central-force model fails to give an adequate description of the observed absorption spectrum, and some improvement is required.

There is good reason to believe that the silver/chlorine ion bond has important noncentral components since the elastic constant C_{44} is much less than C_{12} for silver chloride.[43] The result of a calculation in which both the central and noncentral nearest-neighbor force constants of the silver impurity were varied is shown by full curve in Fig. 7. This reproduces all the features of the experimental curve using physically reasonable force-constant changes. In particular, the central force constant is increased by about 6%, in marked contrast to the 50% decrease in this force constant required above when the effects of noncentral forces were not included. This result is in qualitative agreement with the fact that the compressibility of silver chloride is smaller than that of sodium chloride, while the lattice constants of the two crystals are similar.

Using model II, it was not possible to fit both the peak position of the silver resonance and its intensity relative to that of structure towards higher energy. The best fit was obtained with the curve shown in Fig. 7, and this is compared with the experimental result in Fig. 8.[44] The resonance-mode peak could be shifted towards lower energy by decreasing either the central- or the noncentral-force constants, but in each case this was accompanied by a rapid increase in its intensity, while that of the high-energy structure remained essentially unchanged. The calculated energies of the three peaks in the region of the acoustic phonon critical points are within 3% of the experimental values, which is a considerable improvement over the result obtained previously using the phonons of Caldwell and Klein.[1] The shoulder at 155 cm^{-1} occurs in the calculated curve as a peak at 151 cm^{-1}. The failure to resolve this in the experimental curve may be due to errors introduced in subtracting the background absorption of the pure crystal which, even at liquid-helium temperature, is rising steeply in this region.

2. Lithium

For the lithium impurity we have been unable to obtain a satisfactory fit to the experimental data shown earlier in Fig. 1. Using model I it was possible to predict the resonance-mode absorption at 44.5 cm^{-1}, assuming a decrease of 96% in the nearest-neighbor central-force constant, but its peak absorption constant was overestimated by a factor of almost 200 (for a value of $e^*/e=0.74$). In addition the calculated curve failed to reproduce the strong absorption towards higher energy, showing only weak peaks at 134 and 153 cm^{-1}.

From the rigid-ion pictures discussed in Sec. IV B, it was anticipated that model IV might be appropriate to the lithium impurity, but this was found to produce only slight improvements over the fit obtained with model I. Using reductions of 95% in the nearest-neighbor force constant, and 60% in the nearest-neighbor/fourth-neighbor force constant, the frequency of the resonance mode was given correctly, but its intensity was overestimated by a factor of 300 (for a value of $e^*/e=0.74$). Some improvement resulted in the high-energy region where the calculated curve showed a broad band centered at 110 cm^{-1} together with two sharper peaks at 135 and 152 cm^{-1}. The energies of these agree fairly well with those of the experimental peaks at 114 and 141 cm^{-1} and the shoulder at 154 cm^{-1}. However, the peak absorption constants of the three bands in the theoretical curve were in the approximate ratio 1:3:10, which is in marked contrast with the ratio 1.2:1:1 for the corresponding features in the experimental curve.

The fact that the electronic polarizability of lithium is approximately ten times lower than that of sodium[38] suggests that changes in the defect effective charge may be important for this impurity. However, calculations using model V produced no significant improvements in the fit to the experimental data. The intensity of the 44.5-cm^{-1} peak could be reduced by decreasing the lithium effective charge, but this also reduced the strength of the absorption towards higher energy. With a 96% reduction of the nearest-neighbor central-force constant and a value of $e^*/e=0.1$ for the lithium ion, the intensity of the resonance mode was brought to

[43] W. Hinshaw, J. T. Lewis, and C. V. Briscoe, Phys. Rev. **163**, 876 (1967).

[44] Since the completion of this paper our attention has been drawn to measurements of the far-infrared absorption due to silver in sodium chloride by R. Weber and F. Siebert [Z. Physik **213**, 273 (1968)]. Their results agree well with ours at low frequency, but above 100 cm^{-1} their absorption rises more steeply than ours and shows no structure. This additional absorption suggests the presence of unwanted impurities in their crystals, which were grown in air and not chlorine-treated.

within a factor of 20 of the experimental results, but the calculated absorption towards higher energy was between one and two orders of magnitude too weak.

The failure of theory to predict the intensity of the 44.5-cm^{-1} band may result from only a fraction of the total lithium concentration being present in solid solution. The small lithium ion may be able to diffuse readily in sodium chloride and could thus form aggregate centers. In potassium chloride, lithium has a relatively low activation energy for diffusion,[45] although this comparison could be misleading since it occupies an off-center position at the substitutional site in this crystal.[46] The thermal-conductivity results for sodium chloride showed no evidence of the formation of precipitates, but further investigations of the effects of heat treatment on this system are currently being pursued.

The nearest-neighbor central-force-constant changes required above to fit the resonance-mode frequency are in reasonable agreement with the calculated reduction of 91.4% obtained recently by Takeno using an Einstein oscillator model.[18] However, it is clear from our results for the high-energy region that a more elaborate model is required in order to give a complete description of the far-infrared absorption of the lithium impurity in sodium chloride.

3. Potassium

In the case of potassium the main features of the experimental absorption could be fitted using model I, with the nearest-neighbor central-force constant increased by 19%. This gave the frequencies of the three peaks in the experimental curve to within about $3\frac{1}{2}$%, and their relative intensities were also reproduced well. However, the absolute intensity of the calculated curve was almost an order of magnitude lower than that of the experimental result, requiring an unreasonably high value of $e^*/e=2.55$ to give a satisfactory fit. This discrepancy cannot be accounted for by errors in the chemical analysis of the infrared samples, which had a quoted accuracy of ± 1.2%, and is in the wrong direction to be explained by the formation of precipitates or aggregate potassium centers.

The failure of model I in the present case is probably due to the neglect of changes in the Szigeti effective charge of the defect. The electronic polarizability of potassium is approximately four times greater than that of the sodium ion which it replaces,[38] and for a larger, more polarizable cation defect one expects the defect effective charge to be increased.[36] This effect may be included through model V, and a theoretical curve calculated using this model is compared with the experimental result in Fig. 9. Although the relative intensities of the three experimental peaks are not

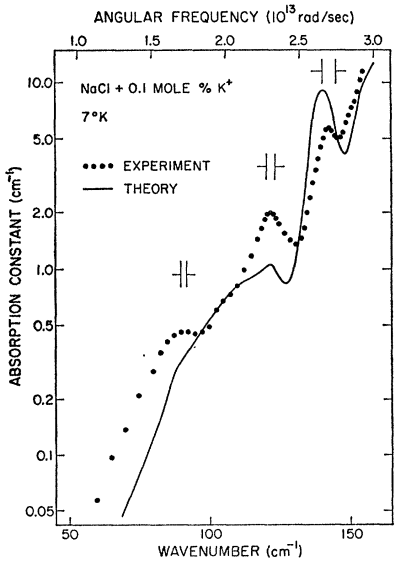

FIG. 9. Comparison of theory and experiment for NaCl:K$^+$, using model V (change in nearest-neighbor force constant, 3000 erg/cm^2, with $e^*/e=2.0$ for the potassium ion and $e^*/e=0.74$ for the host ions).

given as well as by model I, their frequencies are reproduced to better than 1%, and the absolute intensity of the calculated curve is in good agreement with experiment.

For the curve shown in Fig. 9, the nearest-neighbor central force constant was increased by 19%, the same increase required by the best fit with model I, and the effective charge values used were $e^*/e=2.0$ for the potassium ion, and the sodium chloride value of $e^*/e=0.74$ for the host ions. Since only the nearest-neighbor central-force constant is changed in model V, the radiation couples to a vibrational configuration consisting of a relative motion of the defect and two of its nearest neighbors along the line joining them. With the above value of the defect effective charge, that of the two nearest-neighbors is $e^*/e=-1.37e$ [see Eq. (14) of Ref. 26], indicating that the electron distributions of the large potassium ion and the nearest-neighbor chlorines are coupled strongly to the chlorine-ion motion and are influenced less by motion of the central potassium ion. On a shell-model picture this situation would be described by a decrease of the potassium-ion shell charge, together with an increase of the nearest-neighbor chlorine-ion shell charges.

4. Fluorine

In Sec. IV B we indicated that model IV should be appropriate for the fluorine impurity in sodium chloride. The calculated absorption using this model is compared with that obtained using model I in Fig. 10. In both cases the nearest-neighbor central-force constant was adjusted to give the resonance-mode peak at the observed position of 59.5 cm^{-1} at 7°K, and, for the

[45] R. C. Hanson, Bull. Am. Phys. Soc. 13, 902 (1968).
[46] See the discussion of Sec. I C 2 of Ref. 10, and references therein.

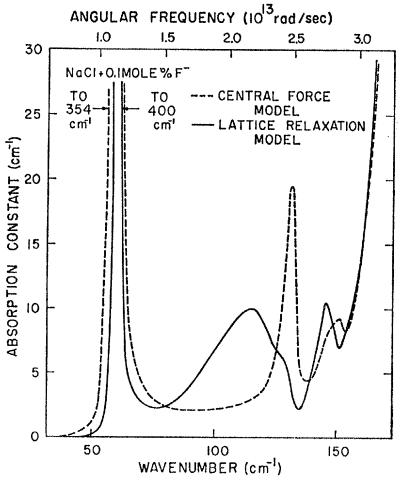

FIG. 10. Calculated absorption of NaCl:F⁻, with $e^*/e=1.0$. (Full curve, model IV with change in nearest-neighbor force constant, −14 045 erg/cm², and change in nearest-neighbor/fourth-neighbor force constant, −8000 erg/cm²; dashed curve, model I with change in nearest-neighbor force constant, −14 500 erg/cm².)

lattice-relaxation model, the nearest-neighbor/fourth-neighbor force constant was adjusted to give the best fit to the high-energy peaks in the experimental curve (see Fig. 2). From Fig. 10 (see also Ref. 1) it is evident that model I cannot account for the observed fluorine absorption, and that effects of the inward relaxation of the nearest-neighbor sodium ions must be considered. When this is done using model IV good agreement with experiment is obtained; this is illustrated in Fig. 11. The peak positions of the two high-energy bands are within 2½% of the experimental result and, as was the case for the silver impurity, the best fit was obtained with a value of $e^*/e=1.0$. The force-constant changes used, a decrease of approximately 90% in the nearest-neighbor force constant together with a 50% decrease in the nearest-neighbor/fourth-neighbor force constant, are consistent with the arguments based on a rigid-ion picture of the fluorine defect given in Sec. IV B.

5. *Bromine*

For the bromine impurity a moderately good fit could be achieved using a simple mass-defect model, with no force-constant changes. The energies of the experimental peaks at 117 and 140 cm^{-1} were reproduced to within 3%, while that of the 85-cm^{-1} peak was underestimated by about 5%. This represented a significant improvement over the fit obtained using the Caldwell and Klein phonons which required a decrease of 13% in the nearest-neighbor central-force constant of the bromine ion,[1] a result which is inconsistent with the larger size of this defect compared with that of the chlorine ion which it replaces. A slight improvement in the intensity fit was achieved using model V with a value of $e^*/e=0.7$ for the bromine ion, but the energies

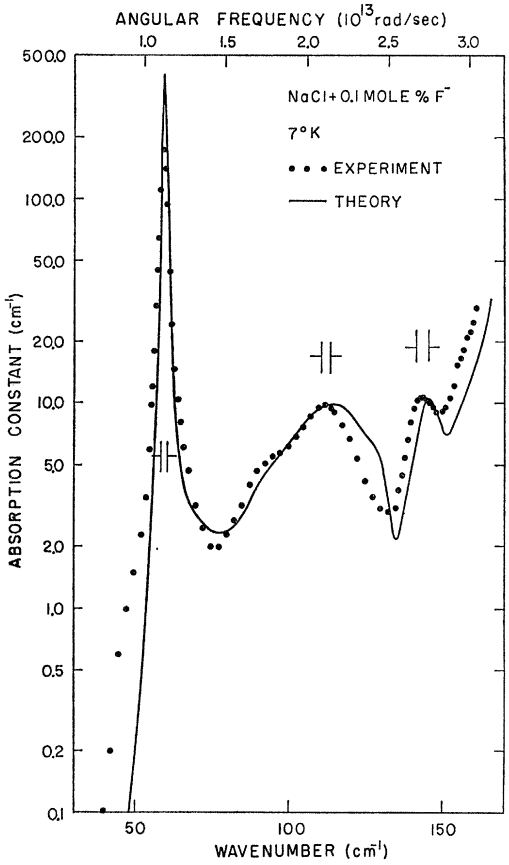

FIG. 11. Comparison of theory and experiment for NaCl:F⁻, using model IV with parameters as for full curve of Fig. 10.

of the three peaks in the calculated curve remained unchanged. This value of the defect effective charge is close to that of sodium chloride, as might be anticipated since the electronic polarizability of bromine is only 40% greater than that of chlorine.[38]

However, a more satisfactory fit to the bromine data was obtained using model III with a value of $e^*/e=0.75$; this is shown in Fig. 12. The inclusion in this model of next-nearest-neighbor forces has two main effects. First, the peak position of the low-energy band is brought to within 2% of the experimental value. Secondly, its intensity relative to that of the two peaks towards higher energy is decreased, giving better agreement with experiment.

6. *Iodine*

In the case of the iodine impurity a reasonable fit to the experimental data was obtained using model I. With an increase of approximately 10% in the nearest-neighbor central-force constant, the main features of the experimental curve were reproduced, but the peak position of the low-energy band at 71 cm^{-1} was shifted towards lower energy by about 3%. As for bromine, the fit was improved by including the effects of next-

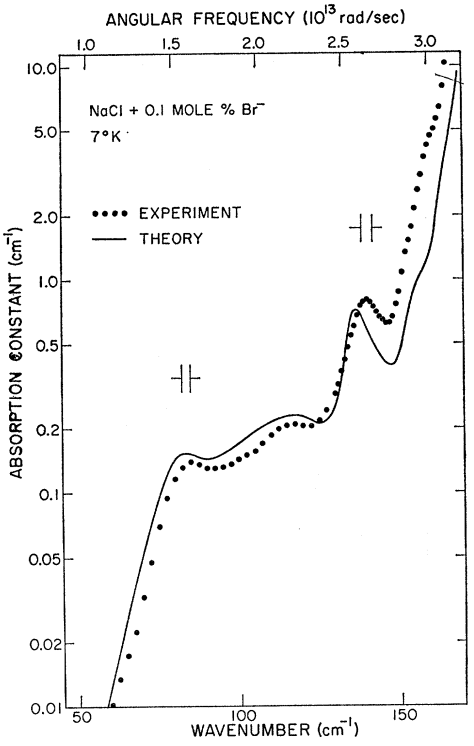

FIG. 12. Comparison of theory and experiment for NaCl:Br^-, using model III with $e^*/e=0.75$. (Change in nearest-neighbor force constant, equal to change in next-nearest-neighbor force constant, 600 erg/cm².)

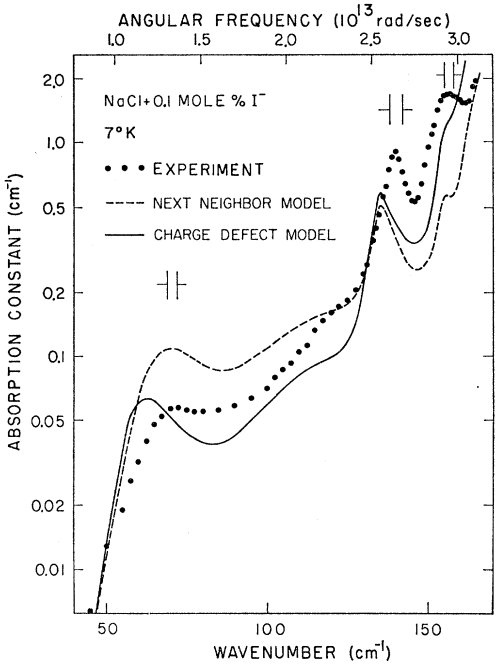

FIG. 13. Comparison of theory and experiment for NaCl:I^-. (Full curve, model V with no change in nearest-neighbor force constant, and $e^*/e=0.55$ for the iodine ion and $e^*/e=0.74$ for the host ions; dashed curve, model III with change in nearest-neighbor force constant, equal to change in next-nearest-neighbor force constant, 3000 erg/cm², and $e^*/e=0.6$.)

nearest-neighbor interactions, and a fit to the experimental results using model III, with a value of $e^*/e=0.6$, is shown by the dashed curve in Fig. 13. Although the peak positions of the absorption bands in the calculated curve agree with experiment to within better than about 3%, the intensity agreement is poor. The intensity of the 71-cm^{-1} band could be reduced by increasing the nearest-neighbor force constant, but this resulted in a rapid decrease, and the eventual disappearance, of the 156-cm^{-1} peak. The intensity of this latter band could be increased by decreasing the next-nearest-neighbor force constant, but this also shifted the 71-cm^{-1} band towards lower energy, and the calculated curve shown in Fig. 13 represents the best compromise fit to the experimental result.

A considerable improvement in the intensity agreement was achieved by using model V. As for the potassium impurity, effective charge effects are expected to be important for iodine since its electronic polarizability is more than a factor of two greater than that of the chlorine ion which it replaces.[38] For a larger, more polarizable anion defect the effective charge should be decreased and this is confirmed by the values of $e^*/e=0.55$ for the iodine ion, and $e^*/e=0.74$ for the host ions which gives the best fit to the experimental data shown by the full curve in Fig. 13. Except in the region of the 156-cm^{-1} band, the shape of the calculated absorption was relatively insensitive to changes in the nearest-neighbor central-force constant, and the curve shown in Fig. 13 was obtained with no change in this force constant. Increasing the nearest-neighbor force constant, which would be physically reasonable for the large iodine impurity, resulted in a rapid decrease of the 156 cm^{-1}, but had almost no effect on the peak position of the low-energy band, which occurs almost 10% lower in energy than the experimental peak. From the two theoretical curves shown in Fig. 13, it is evident that both effective charge effects and next-nearest-neighbor interactions are important for the iodine impurity in sodium chloride.

VI. CONCLUSIONS

The results of this study show that, in general, it is necessary to extend the nearest-neighbor central-force-constant model (model I of Sec. IV B) in order to account for the far-infrared absorption due to chemical impurities in the sodium-chloride lattice. For five of the six chemical impurities studied simple extensions of this model resulted in good agreement with the experimental data over a broad frequency range. The results for the strongly perturbing silver, lithium, and fluorine defects indicate the importance of considering both resonance-mode absorption and band-mode absorption in the acoustic phonon critical point region in calculations of far-infrared impurity-induced spectra. In

the case of silver it was necessary to include the effects of noncentral forces to obtain a satisfactory description of the resonance-mode absorption and the high-energy structure, while for fluorine this was achieved only when the effects of inward relaxation of the nearest-neighbor sodium ions were included.

For all six chemical impurities studied there was a lack of good agreement between theory and experiment at the high-energy limit, close to the reststrahlen frequency. This may be due in part to errors introduced in subtracting off the steeply rising background absorption of the pure crystal, as was discussed in connection with the silver data in Sec. V B 1. In addition, errors in the acoustic-phonon energies close to the reststrahlen frequency would result in corresponding inaccuracies in the T matrix appearing in Eq. (9). These in turn would be amplified by the factor $\omega/(\omega_0^2-\omega^2)^2$, which is a rapidly rising function of frequency in this region, and could give rise to large discrepancies in the calculated absorption constant.

Although the defect models used in this work gave good agreement with experiment on the whole, it is clear that some improvements can be made. The availability of low-temperature neutron data for sodium chloride would be useful in providing a detailed check of the phonon-dispersion curves calculated in Sec. III. The chlorine isotope-induced absorption provides a direct test of the chlorine-ion density of states, but is not sensitive to minor details of the phonon-dispersion curves. In addition, it contains only a limited number of peaks in the acoustic-phonon region, and it was not possible to make unambiguous assignments of these to specific van Hove singularities. From the theoretical fit to the isotope data it is evident that the recalculated phonons are considerably better than those of Caldwell and Klein.

Another improvement would be the use of more elaborate defect models, and in particular the addition of changes in the defect effective charge to all of the mass–force-constant models described in Sec. IV B. The approximation of models I–IV, that the defect effective charge is the same as that of the neighboring ions, worked reasonably well for the silver, fluorine, and bromine impurities, although the necessity of treating the Szigeti effective charge as an arbitrary parameter in order to obtain good intensity agreement was not altogether satisfactory. However, the values of e^*/e required to obtain a good fit to the experimental results using models I–IV showed a behavior consistent with the size and polarizabilities of the various impurities. For example, the three halide-ion impurities studied, whose ionic radii[37] increase with increasing atomic number, showed the expected decrease in the values of their respective Szigeti effective charges, namely, 1.0, 0.75, and 0.6.

The success of model V in accounting for the intensity dependence of the potassium and iodine spectra, together with the partial success of model IV in explaining the lithium results, leads us to speculate that a model incorporating both changes in the defect effective charge, and lattice-relaxation effects might be appropriate to the lithium impurity in sodium chloride. It is hoped that in future work a model of this form, together with the further experiments mentioned in Sec. V B 2, will result in a more complete understanding of the lithium system.

ACKNOWLEDGMENTS

We would like to thank V. G. Mossotti and members of his analytical staff for their analysis of some of the crystals used in this investigation. Thanks also go to J. Gould for performing some of the early optical-absorption calculations.

The computer program used for the shell-model calculation described here was originally written by R. A. Cowley and the Chalk River group, and was translated into FORTRAN language by T. Timusk and R. F. Caldwell. All calculations were performed on the IBM 7094-1401 computer installation in the Department of Computer Science at the University of Illinois.